


RESEARCH ARTICLE

Experimental studies on the Hartmann tube

E. Rathakrishnan 

Department of Aerospace Engineering, Indian Institute of Technology Kanpur, Kanpur, India
Email: erath@iitk.ac.in

Received: 10 December 2023; **Revised:** 12 March 2024; **Accepted:** 18 March 2024

Keywords: Hartmann tube; sonic jet; expansion level; screech; oscillation; mode; frequency

Abstract

The effect of tube depth, the separation distance between the tube and nozzle exit, and the nozzle pressure ratio on the characteristics of the flow coming out of the Hartmann tube was studied experimentally. The configuration used in this work consists of an underexpanded sonic jet emanating from a convergent nozzle directed into a closed-ended cylindrical tube of the same diameter (D) as the nozzle exit. The nozzle was operated at two levels of underexpansion corresponding to nozzle pressure ratio (NPR) 3 and 5. The distance (S) from nozzle exit and tube inlet was varied from $0.4D$ to $4D$. Discrete high-amplitude tones (the jet regurgitant, JRG) were produced, only at certain (periodic) intervals (near the shock-cell terminations) of spacing for NPR 3, while for NPR 5 the JRG tones are produced at all points beyond the first shock-cell. For locations other than these, high-frequency tones (screech mode) were observed. The connection between the jet structure and operating modes revealed that the location of standoff shock ahead of the tube with respect to the jet structure plays a dominant role in the observed ‘modes’ rather than the nozzle tube separation. The results reveal that the frequency response of longer tubes in JRG mode approaches their quarter wave frequencies. The high-frequency oscillations observed in the screech mode showed independency with cavity (pipe) depth, contrary to the available literature, the transition between ‘different modes’ oscillation is a function of cavity depth.

Nomenclature

NPR	nozzle pressure ratio
P_o	settling chamber pressure
P_a	atmospheric pressure
P_p	pitot pressure
D	diameter of the nozzle
S	nozzle-cavity separation
L	cavity depth
JRG	jet regurgitant mode
x	axial direction of the jet

1.0 Introduction

High-power acoustic generators with output from low audio frequency to ultrasonic are of value in some divisions of technology. For instance, high-powered sonic generators have many vital applications in aerospace engineering, including the detection of fatigue failures in airframe and spacecraft components, as well as the precise control of combustion in solid propellant rocket motors. In general, the acoustic generators may be classified as aero-sonic, aeromechanical and electro-mechanical. Aero-sonic generators have no moving components and hence referred to as ‘static’ generators, whereas the aero- and electro-mechanical generators equipped with moving components are called ‘dynamic’ generators.

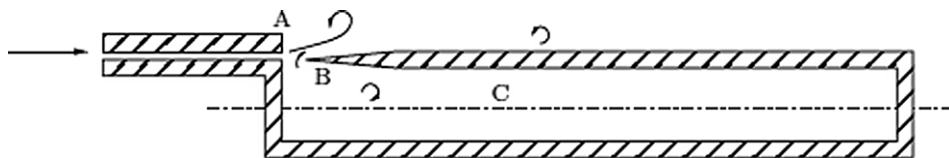


Figure 1. Organ pipe.

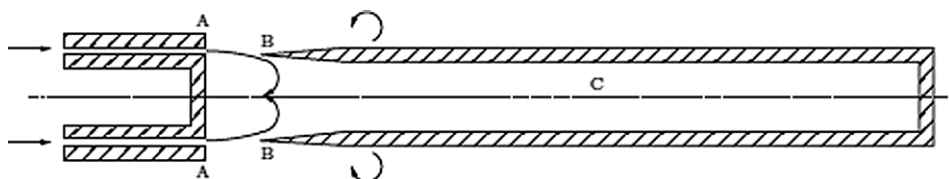


Figure 2. Galton whistle.

The Hartmann, Levasseur and Galton whistle are the well-known static generators. The operation of the Galton whistle and Levasseur whistle depends on subsonic and supersonic edge-tone phenomena [1]. As of now, the precise operating mechanisms of the vortex whistle and the Hartmann whistle have not been fully identified or understood. In the experimental study concerning the variation of stagnation pressure along the axis of a supersonic jet, Hartmann observed that there were specific locations where the pressure-probe assembly experienced high-amplitude oscillations. This discovery sparked further investigations into the oscillations of various enclosed cavities situated within supersonic flows. Since then, though, Hartmann, his co-workers and many others studied this problem. However, so far, no study accounting for all aspects that initiate and maintain the oscillations in the Hartmann tube is reported in open literature.

The whistle depicted in Fig. 1 illustrates a tuned cavity that is stimulated by a low-velocity air jet, forming the fundamental principle for numerous musical instruments. A jet originating from a slit orifice at point A strikes the edge at point B, producing an edge-tone within a specific range of flows, distances between the jet and the edge. The cavity labeled as C in Fig. 1 produces what are known as force edge-tones. However, the output of this device is relatively low. Regarding the Galton whistle, depicted as the upper section in Fig. 1 and possessing rotational symmetry around its longitudinal axis, the acoustic output is notably enhanced.

Quarter-wave resonant excitation in the cavity by a coaxial edge-tone is the cause for this enhancement. Although the acoustic efficiency remains low, this configuration is capable of producing high-frequency sound (Fig. 2). Though, these whistles can experience acoustic power when excitation jets surpass the critical pressure, it should be noted that intense oscillations within the enclosed air column would be caused by supersonic edge-tones. Because of the non-linear nature of the sound consisting of odd- and even-numbered harmonics, these oscillations can no longer be characterised as ‘small perturbations’.

The high-pressure Galton whistle mechanism remains incomplete, owing to the lack of comprehensive data on supersonic edge-tone phenomena. Figure 2 illustrates the commercially successful high-pressure variant of the basic whistle, referred to as the Levasseur whistle. An improved whistle, which incorporates two toroidal cavities and has been experimentally proven to enhance its output, is depicted in Fig. 3. The Hartmann whistle, in contrast to the previous examples, operates differently and for its functionality it is independent of edge-tone phenomena [2]. The open end of the Hartmann whistle is aligned facing a high-speed jet. Gas confined within the cavity exhibit intense turbulent oscillations at one of its resonant harmonic frequencies. This results in the emission of highly concentrated acoustic radiation at discrete frequencies when the velocity of the jet exceeds the speed of sound.

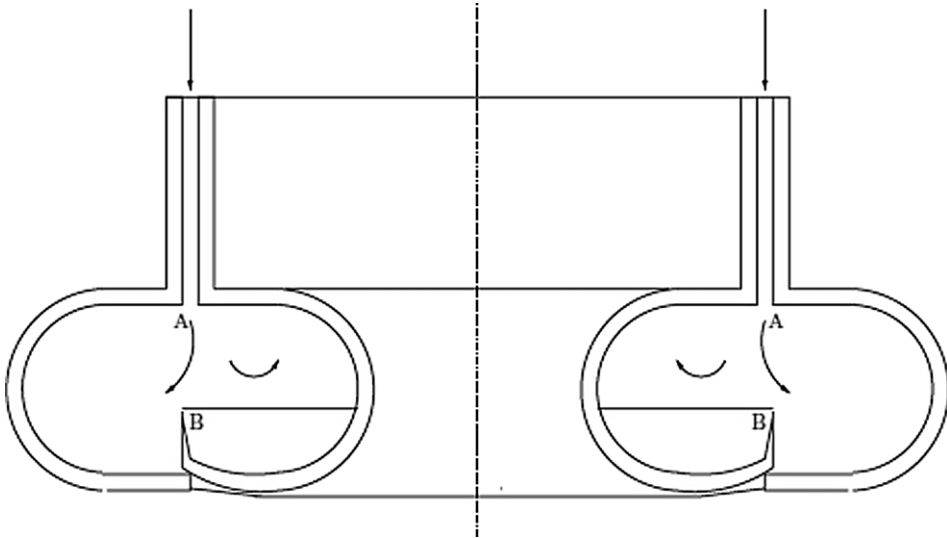


Figure 3. Levavasaeur whistle.

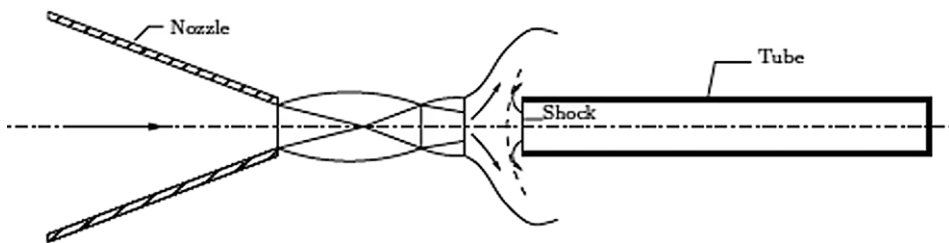


Figure 4. Hartmann tube.

Weak oscillations of the air column can be induced using subsonic jet [3]. However, achieving resonance in this scenario requires precise control, adjustment of the geometric and flow parameters to meet the necessary configuration. The generation of vortices, akin to the edge-tone phenomenon responsible for this type of oscillation is referred to as the jet instability mode. In the case of supersonic flow, these parameters become less critical. Variation of jet-to-cavity distance results in oscillations over a broad range of pressures.

Figure 4 illustrates the cavity designed as a closed, cylindrical resonator with a flat bottom. The length-to-diameter ratio of this resonator can span a wide frequency range, from as low as 0.25 to potentially exceeding 50. Usually the nozzle and cavity are of the same diameter (Fig. 4). When a large Helmholtz resonator is employed as the cavity, frequency typically in the range of 0.5 cycles per second (c/s) or even lower can be achieved. This arrangement is often referred to as the ‘Hartmann pulsator’. Resonant cavities oriented with their orifices facing the flow direction frequently produce high-intensity discrete-frequency sounds. These oscillations share many similarities with those observed in the Hartmann whistle. It is worth noting that this phenomenon seems to be connected to Ramjet instability, commonly referred to as ‘Ramjet buzz’. The pits in some meteorites are a consequence of cavity resonance that occurs as the meteorite travels through the Earth’s atmosphere. The significant amplitude oscillations within these cavities contribute to the expulsion of molten material from the pits [4].

The studies conducted using thick-walled resonant tubes, which were enveloped by substantial heat sinks, often failed to consider the heating effect. Using a thin-walled, 8-mm diameter oscillator, 7 deg.

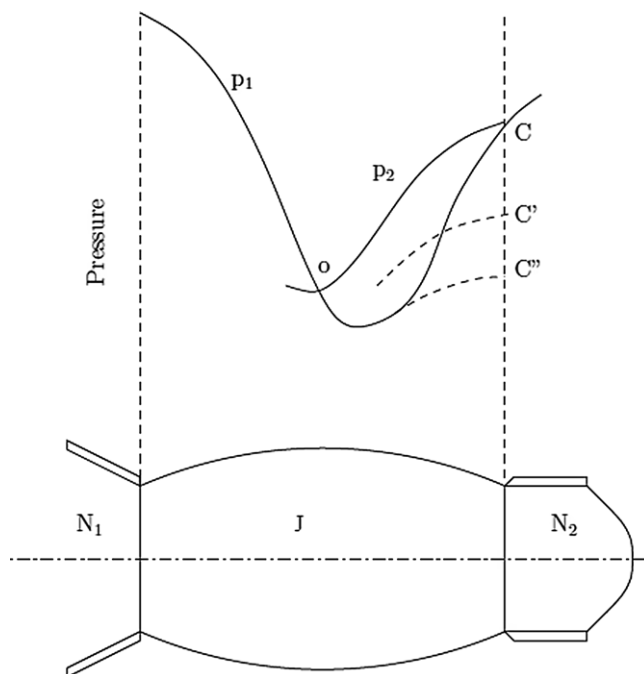


Figure 5. Diagram to illustrate Hartmann's postulated mechanism.

C temperature rise at the base of the cavity was found by Hartmann. Study by Gravitt [5] revealed that the heat generated in the cavity enlarged the cavity cut in wood or paraffin wax. Resonator of this type is also referred to as air-jet generator, gas-jet siren, jet-type vibrator, static siren, etc. [5, 6].

2.0 Literature review

In 1919, Hartmann conducted a series of experiments aiming to analyse the fluctuation of stagnation pressure along the axis of a spatially supersonic jet. The pitot tube experienced intense oscillations, whenever its orifice was positioned in proximity to some specific points within the jet efflux. These oscillations were identified as acoustic in nature, and the wavelength of the emitted sound was found to be dependent on the longitudinal dimensions of the pitot tube assembly. Subsequent experiments employing a large Helmholtz resonator demonstrated that the system oscillates at an exceptionally low frequency. The efflux of the jet directly flows into the cavity, with the external detached shock disc positioned in close proximity to or even within the orifice of the pulsator.

Subsequent experiments carried out by Hartmann involving very small cylindrical cavities showed that flow variations during the resonance of one of these cavities were similar to those observed with the pulsator. This observation led to Hartmann's theory regarding the mechanism behind these 'intervals of instability'. This theory connects these intervals to his investigations into the fluctuation of stagnation pressure along periodic jets, as depicted in Fig. 5 [7]. first, the cavity N_2 initially fills up to reach the equilibrium pressure denoted as C , which corresponds to the pressure at the location of the cavity's orifice; then formation of a supersonic jet from its orifice results when air from the cavity is released by a minor flow disturbance. next, the periodic axial pressure distribution of the main jet (p_1) is suppressed by the disturbances of the cavity flow (p_2). The main jet causes the cavity to become empty until the primary jet once again overcomes the displaced air mass (C'') and refills the cavity, owing to the collision of the secondary jet. Finally, the natural frequency of the cavity, caused by an unspecified wave motion occurring within it, regulates the frequency of this cyclic phenomenon.

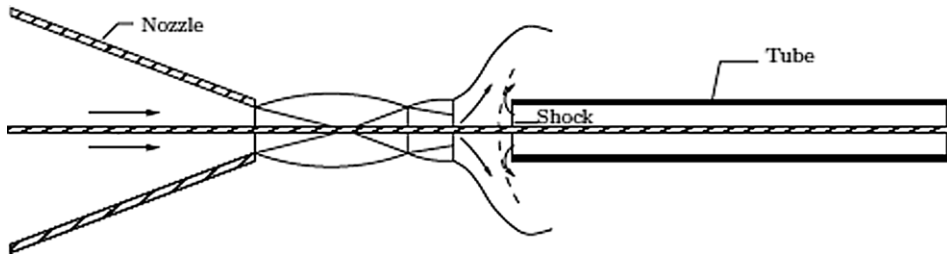


Figure 6. Stem-jet generator.

This partially accurate hypothesis not only explains the observed cyclic flow variations but also highlights the relation between the spatial pressure periodicity of the jets and the occurrence of these ‘intervals of instability’.

Following Hartmann’s research, numerous studies were conducted involving a broad range of modifications to the fundamental assembly. Alterations to reflecting surfaces around the nozzles and cavities are the modifications usually done. Researchers explored various approaches such as jets and cavities with rectangular or annular cross-sections, with different nozzle profiles for the cavities, to enhance the output. Among the configurations explored, one of the most successful is the ‘stem-jet’ as depicted in Fig. 6, in which an axial rod extends through the jet stream from the cavity to the nozzle [7].

Hartmann’s research indicated that the highest achievable aero-acoustic efficiency for the fundamental whistle design was approximately 6% when the diameter and length of the cavity are equal. However, this efficiency decreased as the excess pressure increased, reaching its maximum around 1.5 atmospheres. Furthermore, the efficiency was optimised at specific nozzle-to-cavity separation distances.

Savory [8] conducted experiments involving the construction of various whistle configurations, focusing on the impact of incorporating destabilising devices into the jet stream ahead of the cavity. Borisov’s [1] findings suggested that for maximising acoustic efficiency and enhancing the performance of the whistle. This study showed that the diameter of the cavity should match the widest diameter reached by the cell structure of the jet efflux. Brun and Boucher [3] developed high-powered generator for industrial applications. The ‘multi-whistle’ developed by them had the configuration of multiple Hartmann whistles arranged within the throat of an exponential horn. These whistles were supported by an additional resonant cavity. Gravitt’s [5] efforts aimed to establish a comprehensive theory that could explain the frequency response of a given resonator.

Thompson [9] studied a non-acoustic examination of the Hartmann whistle, in conjunction with flow visualisation, with the aim of documenting the fluid dynamics features associated with the phenomenon of temperature increase within the cavities. This investigation with fully expanded and moderately underexpanded jets revealed that the oscillations within the cavity were fundamentally similar in both scenarios. Wave diagram was used and based on the phases observed in a cycle of the oscillation developed a theory to predict the maximum attainable temperature at the end wall of the cavity. Morch [10] conducted a comprehensive investigation of the Hartmann whistle, reporting both theoretical and experimental results.

Smith and Powell [11] attempted a qualitative theory to explain the mechanism of oscillations in the tube based on his experiments with a Helmholtz resonator. By observing the cycle of oscillation in this so-called ‘Hartmann pulsator’ supplemented by interacting jet studies, he proposed a ‘bistable’ condition for the oscillations.

The other notable works in the theoretical development of the mechanism are due to Brocher et al. [2] and Kawahashi and Suzuki [12]. Brocher employed a simplified wave diagram and a gas-speed/sound-speed diagram to provide a reasoned explanation of how the oscillations initiate and progress to a limiting value within a resonance tube. The condition under which the oscillation amplitude tends toward a

limiting value is characterised by the presence of a low-pressure region at the inlet of the cavity. When this condition is met, the jet is entirely absorbed by the tube during the compression phase of the cycle. He demonstrated that with such a condition it is also possible to obtain oscillations in the case of subsonic flow and correctly expanded supersonic flows. Kawahashi and Suzuki [12] approached the problem of cavity oscillations by extending the method developed by Morch [10] and drew the conclusion that the origin^[SEP] of air column oscillations in the HS tube excited by a moderately underexpanded air^[SEP] jet issuing from a convergent nozzle lies in a negative resistance and that the air column oscillations can be produced within wider ranges than Hartmann's 'intervals of instability'.

The most cited paper in the current works on the Hartmann tube is Sarohia and Back [13]. The resonance tube flows based on their study are classified into (i) Jet instability mode^[SEP] (ii) Jet regurgitant mode^[SEP] (iii) Jet screech mode. ^[SEP] They explained the individual modes based on flow visualisation techniques as follows.

Jet instability mode: This mode of resonance tube operation occurs only for a subsonic jet, i.e. $NPR < 1.9$ over a wide range of spacing S/D . In this mode, the oscillation frequency of the jet flow was observed to fall within a relatively narrow range of non-dimensional frequency parameters ($f d/V$), typically ranging from 0.3 to 0.4, where V represents the mean velocity at the nozzle exit. As the nozzle pressure ratio (NPR) was elevated beyond the threshold of 1.9, a periodic shock structure became evident within the jet flow situated between the nozzle exit and the inlet of the tube.

Jet regurgitant mode: The jet regurgitant mode, as observed by other researchers (e.g. Thompson [9]), involves the periodic intake and expulsion of the jet flow by the tube, occurring at the fundamental resonance frequency of the tube.

Jet screech mode: The transition from JRG to screech mode as postulated by them occurs for spacing less than the free jet shock location. It appears however (from the current study, also from the implication of the 'bistable' theory put forward by Smith and Powell [11]) that this is not a correct quantity to be qualified as a criterion for the transition.

The progress made thereafter in understanding the phenomenon is relatively slow except for a few works by Jungowski and Grabitz [14] (worked on the planar Helmholtz resonator, to support the relaxation hypothesis. In essence this theory is similar to that of Morch [10]), Iwamoto and Dekker [15] (attempted hydraulic analogy for the phenomenon), Chang and Lee [4] (for some numerical experiments on the JRG) etc.

However, there is recently much emphasis being put on the studies from the application point of view. The studies are mainly directed toward understanding the parametric dependence of the tube so as to characterise the tube for the construction of a powered resonator configuration. Sarpotdar et al. [16] performed directivity studies. Development is also in progress to use the Hartmann tube fluidic actuators for high-speed flow control (Kastner and Samimy [17]). Thomas, et al. [18] studied the role of non-circular jets in the performance of Hartmann whistles. But this study focuses mainly on the orifice effect on the sound level and not on the mechanism responsible for the nature of the whistle from the cavity. Recently Solomon et al. [19] reported controlled mixing of fuel with fast-moving air is a challenging physical problem relevant to hypersonic systems. With a focus on improving mixing at extreme flow conditions, this paper presents a fundamental study of a novel, high-speed, pulsed-coflow system integrated with ultrahigh-frequency actuators (11–20 kHz).

A series of experiments and theoretical analyses aimed at assessing the thermal energy balance within the system with the assumption that heat gain achieved from viscous dissipation in the shock wave. These studies attempted to ascertain the achievable maximum temperature for a given resonant cavity. In spite of these studies the acoustic source of high amplitude and high frequency for receptivity studies on the shear layer of the jets and its control continues to be a black box.

Having realised the problems with standard loudspeakers and sound (signal) generators, an alternative for a wide range of amplitude and frequency combinations without much loss of functionality was planned for the study. The Hartmann tube is found to be a promising choice, as its potential was cited in a vast amount of literature recently. However, based on the literature on the Hartmann whistle, it is clear that our current understanding of this complex phenomenon needs further investigation. Even a concise

experimental examination of a typical whistle brings to light numerous questions about its properties that, as of now, have yet to be fully addressed.

As Smith and Powell [11] describe, one of the lingering challenges that remains to be solved pertains to the mechanism responsible for initiating and sustaining the oscillations in the Hartmann whistle. Why do regions in which the flow is stable separate the ‘intervals of instability’? Why do the oscillations start and cease instantaneously, rather than growing to a maximum and falling off according to some exponential law? How does a destabilising trip aid the generation of oscillations? Is there more than one mechanism whereby oscillations are driven, and if so, are they independent of each other, or are several types of instability phenomena simultaneously in evidence? This study is limited to understanding the effect of control parameters on the behaviour of the tube.

3.0 Experimental setup

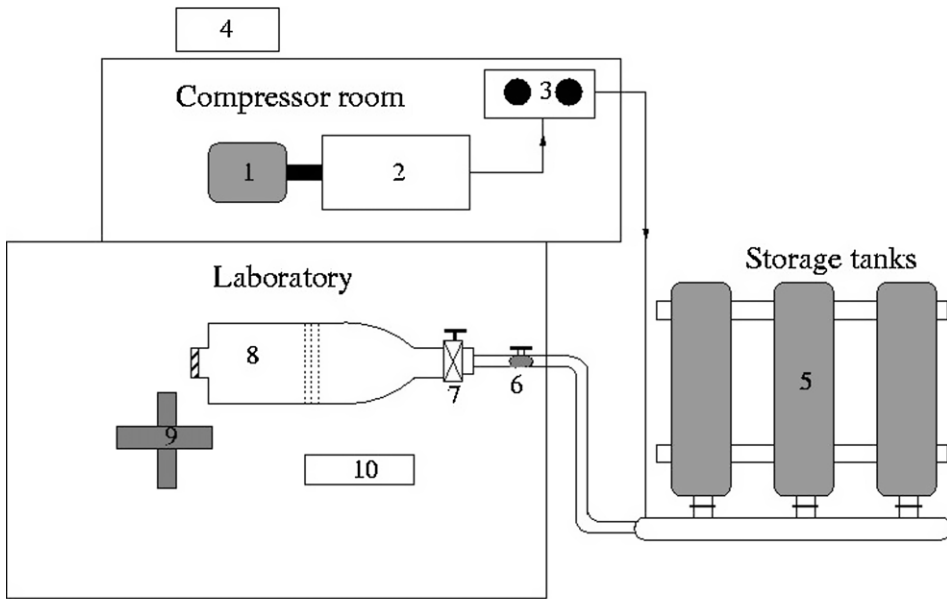
The experiments for the current study are carried out at the high-speed aerodynamics laboratory of the Department of Aerospace Engineering, Indian Institute of Technology Kanpur. The Hartmann Sprenger oscillator construction used for the present investigation consists of a convergent nozzle of exit diameter 10 mm the jet from which is directed against a cylindrical cavity of the same diameter. Three large storage tanks of a combined capacity of 3,000 ft³ maintained at a storage pressure of about 15 bar supply the compressed air to the settling chamber whose pressure can be controlled by a pressure-regulating valve. Plastic tubing connects the settling chamber and entrance piece of the nozzle. The entrance piece has a wire mesh incorporated near the tube end to minimise swirl in the flow that might have resulted from the bend of the connector tubing. A length of about 150 mm is provided for any disturbances in the flow to attenuate and so as to provide uniform flow at the nozzle exit. A provision is made to place a pitot tube inside the entrance piece to record the stagnation pressure.

The settling chamber pressure is also recorded through another pitot tube so that the difference between these two pitot pressures gives an estimate of the losses because of the connector tubing. Figure 7 shows the air supply system and various piping. The cavity is mounted on a platform, which can be moved towards or away from the nozzle exit plane and can be locked at any position by means of a screw. This facilitates study of the effect of nozzle-cavity spacing on the behaviour of the H-S tube. A piston-screw type arrangement is made, the head of which acts as the base (end wall) for the cavity. By rotating the screw the tube (cavity) depth can be varied. Also located is a pitot probe at the other end of the piston head that records any leakage of air through the clearance between the cavity casing and the piston head.

4.0 Instrumentation and acquisition

Near-field acoustic measurements were made 25 jet diameter (25D) away from the nozzle exit using a 1/8" G.R.A.S. external polarised microphone and 800B model Larson and Davis sound level meter. The photograph of the Hartmann tube setup^[11] is shown in Fig. 8. The sound level meter has a digital display that reads OSPL. It also has an output port through which the sampled signal from the conditioner unit can be acquired for processing in the PC through the acquisition board. The DAQ device used is NI PCI 6070E, a 12 bit, 1.25 MS/s, multifunction DAQ with software selectable single-ended/ differential modes of operation. It has a bipolar range of 10 V. The acquisition is made through LABVIEW at a sampling rate of 80 KS/s and is programmed in such a way that real-time display of the power spectrum is made available. Differential mode is used for operation and because the signal is of the floating kind, connections are made accordingly (so as to provide return paths to the ground for bias currents).

Pitot probes are used for stagnation pressure measurements at various locations viz. the settling chamber, entrance piece of the nozzle and the cavity aft-end (behind the piston screw). The centre line pressure distribution from the nozzle exit is made using another pressure probe (a pitot rack, actually) that facilitates the alignment of the probe with the nozzle axis. The signal is acquired through net scanner Model No. 9016, pressure scanner. It uses TCP communication to interface with the PC.



- | | |
|---|------------------------------|
| 1. 150 hp induction motor | 6. Gate valve |
| 2. Reciprocating compressor | 7. Pressure regulating valve |
| 3. Activated charcoal filter and Silica gel dryer units | 8. Settling chamber |
| 4. Water cooling unit | 9. Traversing system |
| 5. Storage tanks | 10. Instrumentation desk |

Figure 7. Jet facility.

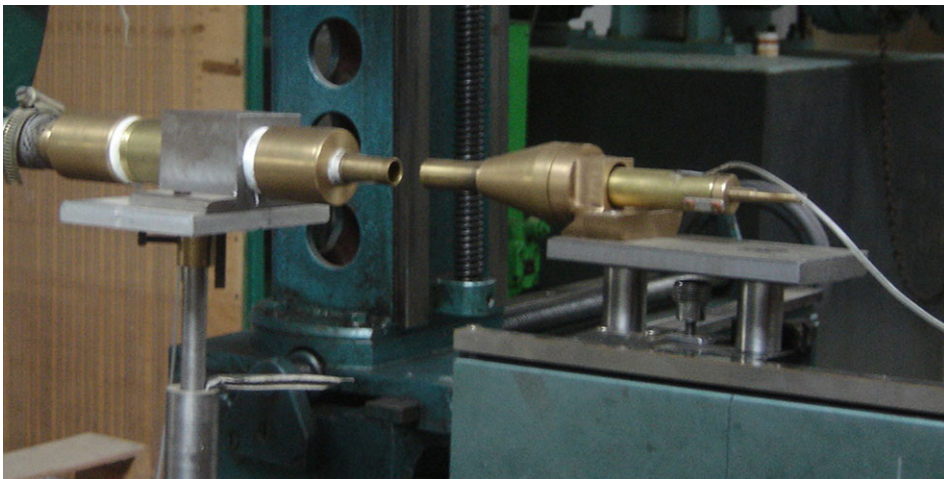


Figure 8. Photographic view of the nozzle and Hartmann tube.

A barometer and mercury thermometers were used to record the day-to-day variations in the ambient pressure and temperature, whenever the tests were made. A shadowgraph system was used to capture the overall features of the free jet shock structure. This system uses a 250-mm diameter concave mirror in conjunction with an air-cooled mercury spark light source. The shadowgraph image was cast on a screen that allowed continuous observation of the field. A digital camera of a frame rate of 25 fps recorded the shadowgraph images of the waves in the flow field.

The microphone fixed on a vertical stand, which was positioned directly above the nozzle exit plane at 25 jet diameters ($25D$) away was used for acoustic measurement. Measurements were performed to capture the spectral content of the signal at various combinations of NPR (the nozzle pressure ratio), L/D (the depth of the cavity to nozzle exit diameter), and S/D (nozzle-cavity spacing ratio). As mentioned previously, the cavity is moved to vary S/D and locked in position with a screw. S/D ratios selected for the present study are 1, 2 and 3. At each of these S/D , the L/D chosen were 0.25, 0.5, 1, 2, 4 and 8. Measurements at some additional combinations; $S/D = 1$, $L/D = 0$; $S/D = 0.5$, $L/D = 1$; $S/D = 1.5$, $L/D = 0.5$; $S/D = 2.5$, $L/D = 1$; $S/D = 3.5$, $L/D = 1$; $S/D = 4$, $L/D = 0$, 1) were also made. However, for comparison, only the aforementioned combinations are used.

The measurements were performed by first locking the cavity at $S/D = 1$, and adjusting the L/D using the screw to 0.25, in this combination of S/D , L/D ; pressure across the entrance section is varied in increments of 3 psig to a pressure of about 93 psig (NPR 1.2 to 6.3). The signal acquired both from the pressure scanner and the microphone was saved to a file (through LABVIEW) for all the NPR of this study. The same measurement was repeated at all values of L/D ratios (0.5, 1, 2, 4, 8). When the set at the given S/D was finished, the procedure was repeated for other nozzle-cavity spacing ($S/D = 2, 3$).

5.0 Centreline pressure measurement

Centreline pressure distribution is made through a pitot rack that had nine probes at 5 mm (half the diameter of nozzle exit) intervals. All the probes were connected to the pressure scanner. The two probes adjacent to the central probe were aligned with the nozzle outer edges when the rack was at $S/D = 0$ from the nozzle so that the central probe's axial alignment with the nozzle centre was ensured. The stagnation pressure value of this (central) probe thus gives the centreline pressure of the jet. The centreline pressure was noted at axial distances in the increments of S/D of 0.1 up to about $S/D = 4$. Because the nozzle is axisymmetric, the pressure profile made across any section has to be axisymmetric. A LABVIEW program is made so that it gives the real-time plot of stagnation pressures across the selected probes of the rack. So the centre alignment is justified when the profile across the jet at any location is symmetric about the mean.

6.0 Shadowgraph visualisation

The shadowgraph images were captured for all the experiments performed i.e., for the free jet as well as the Hartmann tube to supplement the results and for the visual observations of the flow between the nozzle and cavity. A digital camera was used for this purpose. Care was taken to ensure that the mirror, the screen and the test section were in line with each other. This prevents any false images from being cast on the screen because of the misalignment.

7.0 Data accuracy

Storage at higher pressure allowed better control over the pressure of the nozzle within $\pm 0.5\%$. Leakage tests were performed on the probes and also for the cavity-piston clearance leakage. The probes and the cavity setup were operated at full range to check for leaks before the experiments were performed. The pitot rack allowed precise alignment of the probe along the nozzle axis. Because the nozzle is

axisymmetric, the pressure profile made across any section has to be axisymmetric. Differential mode is used for operation and because the signal is of floating kind, connections are made accordingly (so as to provide return paths to the ground for bias currents).

8.0 Results and discussions

The parameters that govern the oscillating characteristics of the Hartmann tube are the nature of the flow (dictated by the nozzle pressure ratio (NPR) and type of the nozzle), cavity depth (L/D), nozzle-to-cavity separation distance (S/D), diameter of the cavity (d/D), shape of the cavity, etc. In the current study, the effect of three of these parameters namely, the cavity depth, the nozzle cavity spacing and the nozzle pressure ratio, are investigated. In the sections that follow, results from the studies on the free jet structure and the effect of the parameters (L/D , S/D , NPR) are presented and discussed at length.

8.1 Free jet studies

Though the exact mechanism by which the Hartmann tube produces tones is not clear, it can be said with sufficient authority that shock cell structure, and static pressure gradient determine whether it can resonate at a particular spacing [11]. In other words, it may be stated that the oscillations of the waves prevailing in the gap between the nozzle exit and the Hartmann tube inlet is the cause for the production of tones.

The NPR, being the parameter that dictates the nature of the flow, was varied from 2.5 to 6, in steps of 0.5. This range for a convergent nozzle implies moderately to highly underexpanded conditions at the nozzle exit. Centreline pitot pressures were measured with a fine hypodermic needle probe connected to a pressure scanner. Since the external diameter of the probe is very small (about 3% of the nozzle exit diameter), the separation region in front of the probe is of very small scale, and the stagnation point is considered to be situated at the probe tip. Hence, the pressures indicated by the scanner related to conditions in a very small region on the axis behind the detached shock at the probe tip.

8.2 The structure of the jet

The jet issuing from the nozzle may be considered as 'choked' as the NPR is > 1.89 . The jet emanating from the nozzle will be correctly expanded sonic jet at NPR 1.89 and underexpanded for $\text{NPR} > 1.89$. In both the case there will be an expansion fan formed at the nozzle exit. The reason for this expansion is due to the relaxation effect for the case of correctly expanded case and due to the combined effect of relaxation and underexpansion for $\text{NPR} > 1.89$. The flow will get accelerated on passing through the expansion fan [20]. The expansion rays on reaching the jet boundary will reflect back as compression waves, in accordance with the gas dynamic theory that wave reflection from free boundary is 'unlike'. This kind of wave reflection will result in the formation of shock cells in the jet core.

The schematic diagram in Fig. 9 presents the waves present in the core of underexpanded jet. Shadowgraph images in Fig. 10 shows the effect of nozzle pressure ratio on the waves present in the core of the jet. With increase of NPR, the expansion rays reflecting from the free boundary, and moving towards the jet axis merge forming a shock. The shocks from opposite direction coming to the jet axis, on reaching the axis, pass through each other and move away from the axis. This shock crossover point remains as a point till NPR 4. For increase of NPR above 4, the shock crossover point tends to become a shock, and for NPR 4.5 and more the crossover point becomes a shock normal to the jet axis. The shock is termed Mach disk (Fig. 10(e)).

The increase in the length of the individual cell with NPR is displayed in Fig. 11. This extracted data from the shadowgraph images also shows a similar variation in the location of the cross-over/Mach disk. The Mach disk grows in size with further increases in NPR.

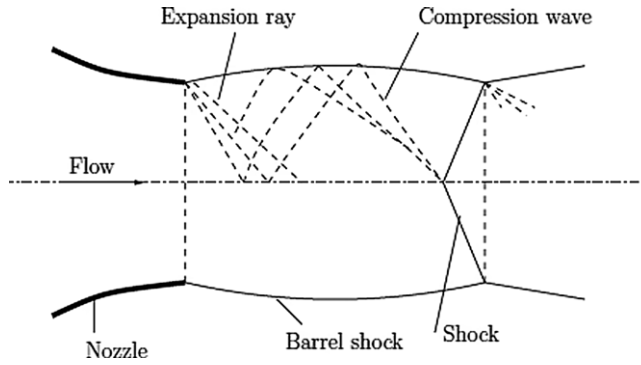


Figure 9. Shock waves in periodic jet efflux.

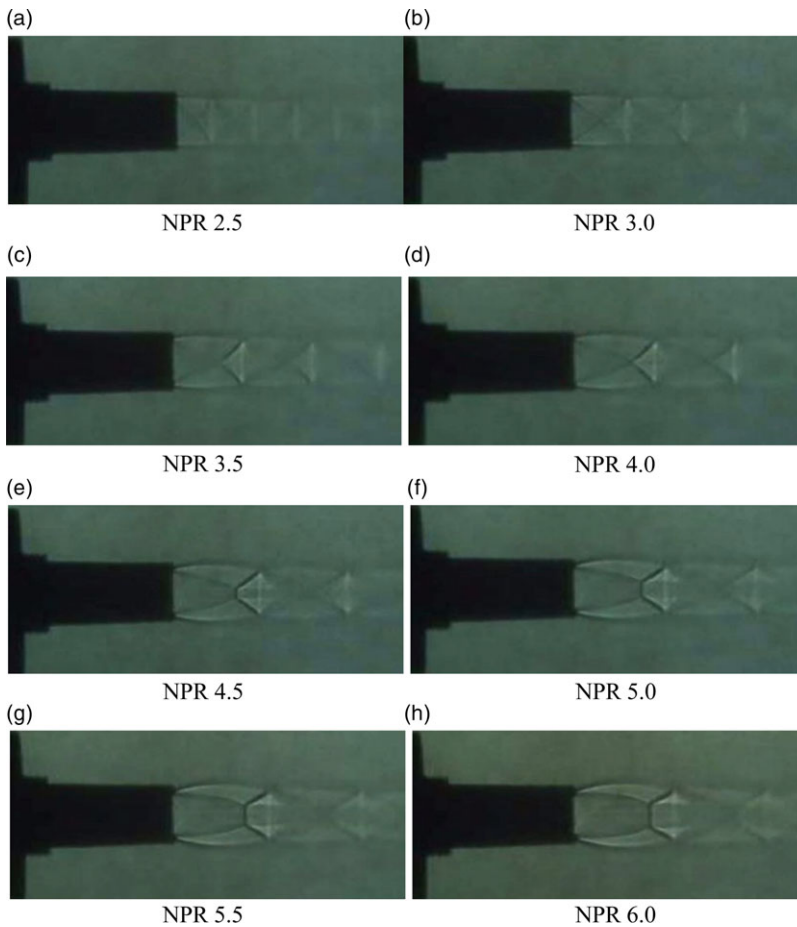


Figure 10. Shadowgraph image of the free jet at different levels of expansion. (a) NPR 2.5, (b) NPR 3.0, (c) NPR 3.5, (d) NPR 4.0, (e) NPR 4.5, (f) NPR 5.0, (g) NPR 5.5 and (h) NPR 6.0.

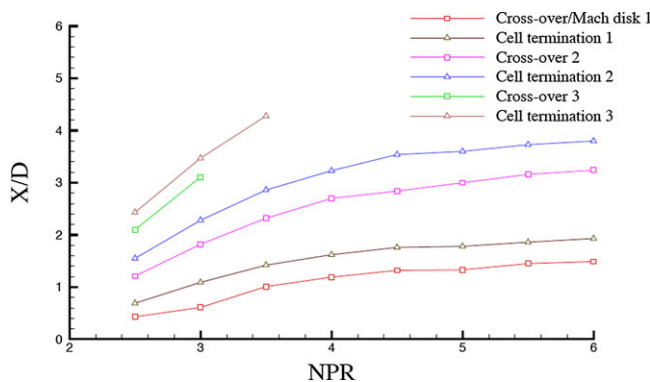


Figure 11. Variation of shock cross-over/Mach disk location and cell termination location with NPR.

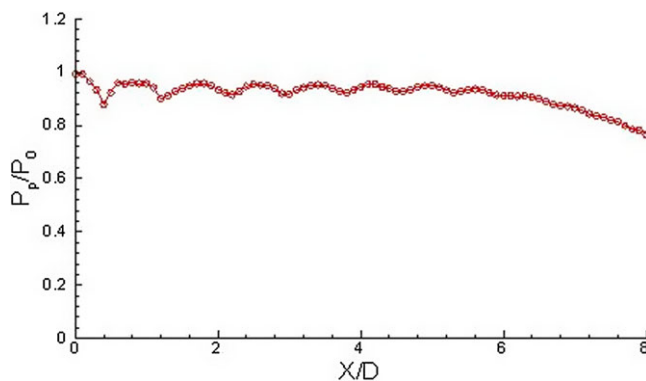


Figure 12. Centreline pitot pressure of free jet at NPR 2.5.

Figures 12-16 show pitot pressure variation along the jet axis, for various NPRs of this study. pitot pressures (indicated on the Y axis) normalised with corresponding stagnation pressure are plotted against the points where the measurements are taken, i.e., X/D starting from 0.1 to 4 moved in increments of 1 mm. It is seen that the amplitude of pitot pressure increases as the NPR increases till NPR 4.5. For NPR > 4.5, the constant pitot pressure region beyond the first minim point (Fig. 15) indicates that the flow becomes subsonic at the Mach disk (which is essentially a normal shock) and continues with constant Mach number some distance downstream of the Mach disk and then accelerates by gaining momentum from the flow with higher momentum coming towards the jet axis. The constant stagnation pressure is attributed to the existence of a subsonic core, and the rise thereafter is due to the gradual mixing with the surrounding flow.

Also, it can be noted that while the shadowgraph pictures distinctly show only the first few cells, with pitot measurements the periodic cell structure can easily be seen to a greater range. Another point is that though the flow loses its strict periodicity beyond NPR 4.5 due to the formation of Mach disk, pitot pressures show repetition in the ‘rise and fall’ in the pressure along the axis which indicates that while recovering from the suffered loss of stagnation pressure due to Mach disk, it continues the cell formation in the subsequent regions.

9.0 The characteristics of the Hartmann tube

To have a preliminary understanding of what happens when a cavity is introduced into the underexpanded jet flow field, the piston screw of the cavity is adjusted to a depth of (L/D = 8). Also, to facilitate

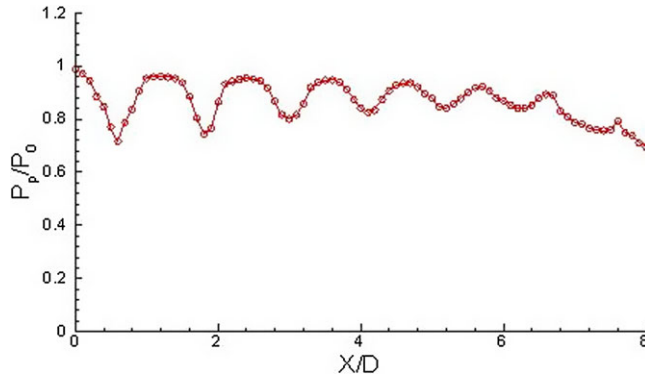


Figure 13. Centreline pitot pressure of free jet at NPR 3.0.

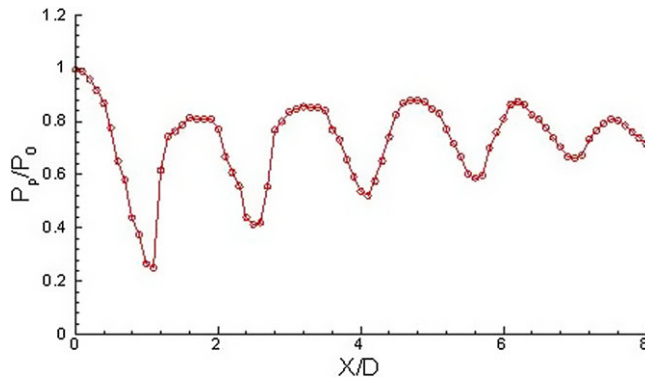


Figure 14. Centreline pitot pressure of free jet at NPR 4.0.

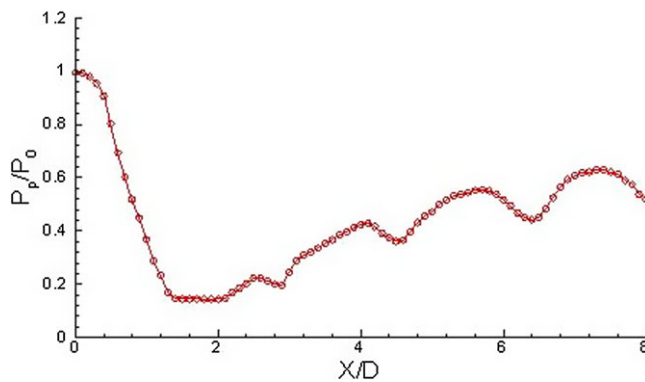


Figure 15. Centreline pitot pressure of free jet at NPR 5.0.

better comprehension of the things involved, it was decided to maintain the flow structure (NPR constant). To observe clearly the effect of the jet structure on the operating characteristics of the tube, NPRs 3 and 5 are selected. As it can be seen from the shadowgraph images and also from the pitot pressure profiles, there is a clear distinction between the structures of the jet at these NPRs. While NPR 3 produces

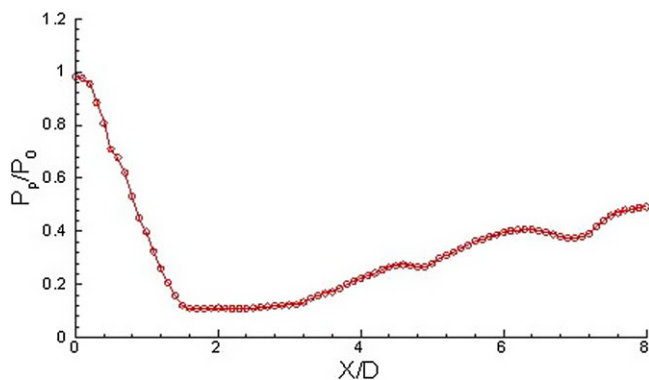


Figure 16. Centreline pitot pressure of free jet at NPR 6.0.

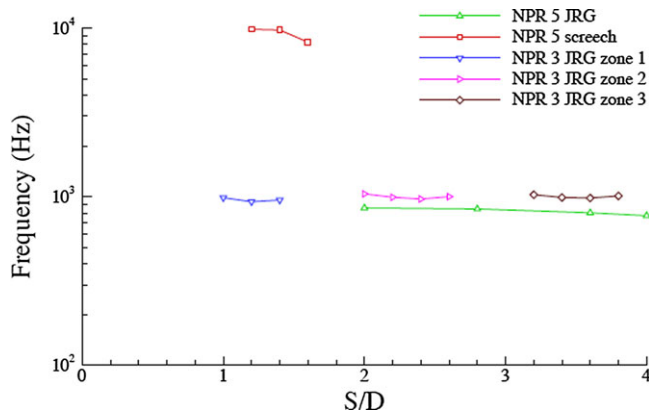


Figure 17. Frequencies corresponding to Maximum amplitude at NPR 3 and 5 ($L/D = 8$).

a moderately underexpanded jet with diamond cell structure, NPR 5 produces a Mach disk, a characteristic of highly underexpanded jets. With NPR and L/D being fixed, the parameter under control is the nozzle-to-cavity spacing (S/D). With the help of a telescopic screw, the cavity is moved towards the nozzle from $S/D = 4$ in decrements of 0.2 to about $S/D = 0.8$.

10.0 The effect of spacing S/D

Figure 17 shows the frequency response of the tube with respect to nozzle-cavity spacing while operating at NPR 3 and 5, with S/D on the x-axis and the frequencies with maximum amplitude on the y-axis. While plotting the figures, because the spectral plot contained many harmonics of the fundamental and since only the high amplitude tones are relevant for the current study, the frequencies corresponding to these amplitudes are only used. In the majority of instances, these are the same as the fundamental frequencies. Also, a cut-off of 130 dB is employed and only those frequencies the corresponding amplitudes of which are above 130 dB are considered.

It is seen that a periodic repetition of a constant frequency band with S/D for NPR 3, between which some high-frequency components (but low amplitude, less than the cut-off) are present. This is expected since the structure of the jet itself is periodic. For NPR 5, the frequency is more or less independent of spacing after about $S/D = 2$. For S/D less than 2, the frequency trend is rising.

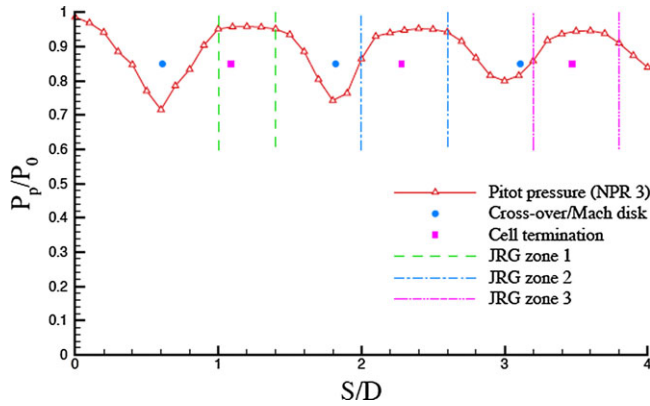


Figure 18. Zonal division of JRG and screech for NPR 3 ($L/D = 8$).

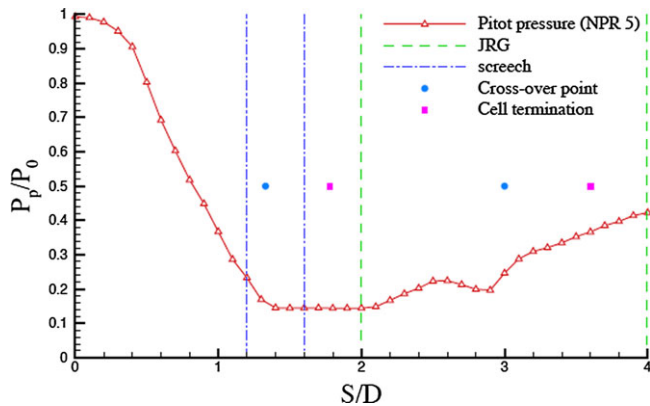


Figure 19. Zonal division of JRG and screech for NPR 5 ($L/D = 8$).

Since the shadowgraph pictures of the free jet were also taken, the cross-over/Mach disk locations and cell lengths are noted for these NPRs, and when the constant frequency bands (as will be termed later, the JRG for the frequencies near quarter wave frequency of the cavity and screech for any higher frequencies) are superimposed on the centreline pressure distribution Figs. 18 and 19 are obtained for NPR 3 and 5, respectively. The implications of these plots will be explained in the following section.

11.0 The modes

Based on his early experiments with a convergent nozzle issuing an underexpanded jet, Hartmann [6, 7] proposed that there exist the ‘intervals of instability’ within which a cavity placed would produce discrete frequency oscillations of the enclosed air column, driven at large amplitudes. These intervals are the regions of rising pressure. Subsequent researchers indicated the possibility of the oscillations even beyond these intervals [12]. Sarohia and Back [13] identified three modes in which the tube can oscillate namely, the jet instability mode, the jet regurgitant mode, and the jet screech mode. Whereas the instability mode is restricted to subsonic flow, the other two occur in supersonic flow (especially underexpanded). Regurgitant mode is identified as high-amplitude oscillations of the flow field driven at almost the quarter wave frequency of the tube while screech is high frequency and comparatively low-amplitude oscillations of normal shock between the nozzle cavity separation region. It was expected that

periodicity in the jet structure should somehow be affecting the JRG-screech repetition as the cavity is moved along the axis of the jet. The oscillations, as Hartmann proposed were expected to occur when the cavity is placed in regions of rising static pressure, the ‘intervals of instability’. The maxima he observed were at the maxima of pitot pressure distribution. Sarohia and Back [13] counters Hartmann’s hypothesis by stating that for the cavity placed beyond the locations corresponding to the termination of the cell, the JRG occurs, while if it is less than so, screech (low-amplitude high-frequency) tone can be observed. This means that the beginning of the zones of instability in the free jet corresponds to the separation between the screech and JRG modes. JRG if the cavity is located in the region of decreasing pressure, screech in increasing pressure.

For NPR 5, as can be seen from Fig. 19, both the claims are valid, i.e. the regurgitant mode occurs at spacing after the first cell location corresponding to the free jet. This also coincidentally happens to be the region of rising pressure. Ironically, no researcher pointed out this subtle difference.

High-amplitude tone associated with periodic inflow and outflow of the jet into the cavity pressure recovery of the central subsonic core with the supersonic stream). But what was observed for NPR 3 is that the spacing at which the regurgitant mode observed was more-or-less centred on the maxima (or near the end of a cell) of the pitot pressure curve. These comments about whether or not JRG occurs are made from the spectral data from which frequencies near the quarter wave frequency of the cavity, are considered to be JRG, while higher frequencies are taken to be screech. Help from the shadowgraph pictures are sought which is shown in Fig. 20 for NPR 3, and Fig. 21 for NPR 5.

The following important observations were made. In what happens to be screech-operating regions (e.g. Figure 20(d)/20(f)), a normal shock appears near the beginning of the shock cell (in the expansion region of the jet) and another shock always appears at the cavity mouth, which is bent towards the cavity. In JRG operating regions (e.g. Figure 20(h)), the flow near the tube mouth is blurred by a shadowy region near the cavity exit. This observation helped distinguish visually, the JRG from screech. The explanation for the observed differences in the images is the following: What basically constitutes JRG is an inflow phase of the jet into the tube and an outflow phase from the tube to the jet. Since the outflow phase is an interaction between the tube outflow (debouching) and jet flow, and also the oscillations are very rapid (about 1000 Hz (for $L/D = 8$) compared to the frame rate of the camera (25 fps)), the interface between the two flows produces a blurred image when captured, as the axial movement of the interface is also large. Screech being very-high-frequency, low-amplitude oscillation of the normal shock in the nozzle-cavity spacing, can easily be identified.

A careful observation of the images (Figs. 10(a)-10(h)) reveals that the spacing between the nozzle cavity is decreased indicates that the conditions at which JRG or screech occur actually depend on the shock standoff location with respect to the jet structure when the cavity is introduced. When this shock is located in the regions of compression, JRG occurs, and if it is in the expansion region (decrease in pressure), screech is observed. So the cavity nozzle spacing is not an important parameter in judging the mode of operation.

12.0 Frequency response of the hartmann tube

Hartmann found that the acoustic output of the whistle is strongly influenced by pressure, cavity location, etc. Hartmann paid attention on the relation between the jet cell structure geometry and the cavity locations where the flow changed from stable (non-resonant) to unstable (resonant) condition. These zones were referred to as ‘intervals of instability’. The wavelengths of the emitted sound over a limited range of distances and cavity dimensions (having lengths more-or-less equal to their diameters, in the range from 2 to 10 mm) were determined. It was found that natural resonant frequencies occurred because of the extreme non-linearity of the oscillations, when nozzle-to-cavity separation was varied. This result led to the erroneous assumption that, throughout the first and subsequent unstable zones the wavelength varied as a linear function of the cavity location (S/D), the frequency decreasing as the spacing increased. However, this assumption was found to be incorrect in the studies with longer cavities. Apart from these surveys, no other detailed investigation of the variations of the sound of a Hartmann

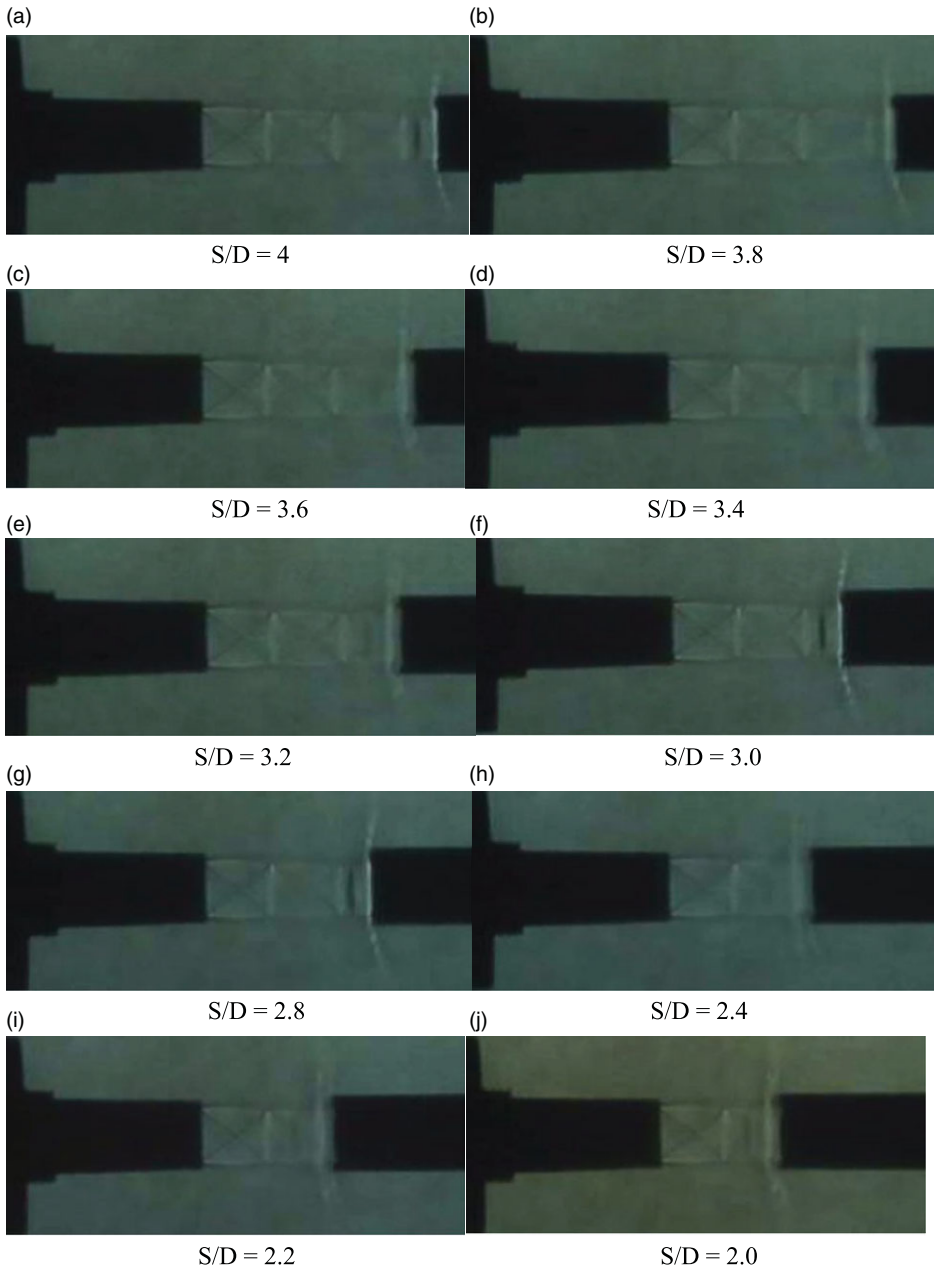


Figure 20. Shadowgraph images for spacing S/D from 4.0 to 0.4 at NPR 3. (a) $S/D = 4$, (b) $S/D = 3.8$, (c) $S/D = 3.6$, (d) $S/D = 3.4$, (e) $S/D = 3.2$, (f) $S/D = 3.0$, (g) $S/D = 2.8$, (h) $S/D = 2.4$, (i) $S/D = 2.2$, (j) $S/D = 2.0$, (k) $S/D = 1.8$, (l) $S/D = 1.6$, (m) $S/D = 1.4$, (n) $S/D = 1.2$, (o) $S/D = 1.0$, (p) $S/D = 0.8$, (q) $S/D = 0.6$ (r) $S/D = 0.4$.

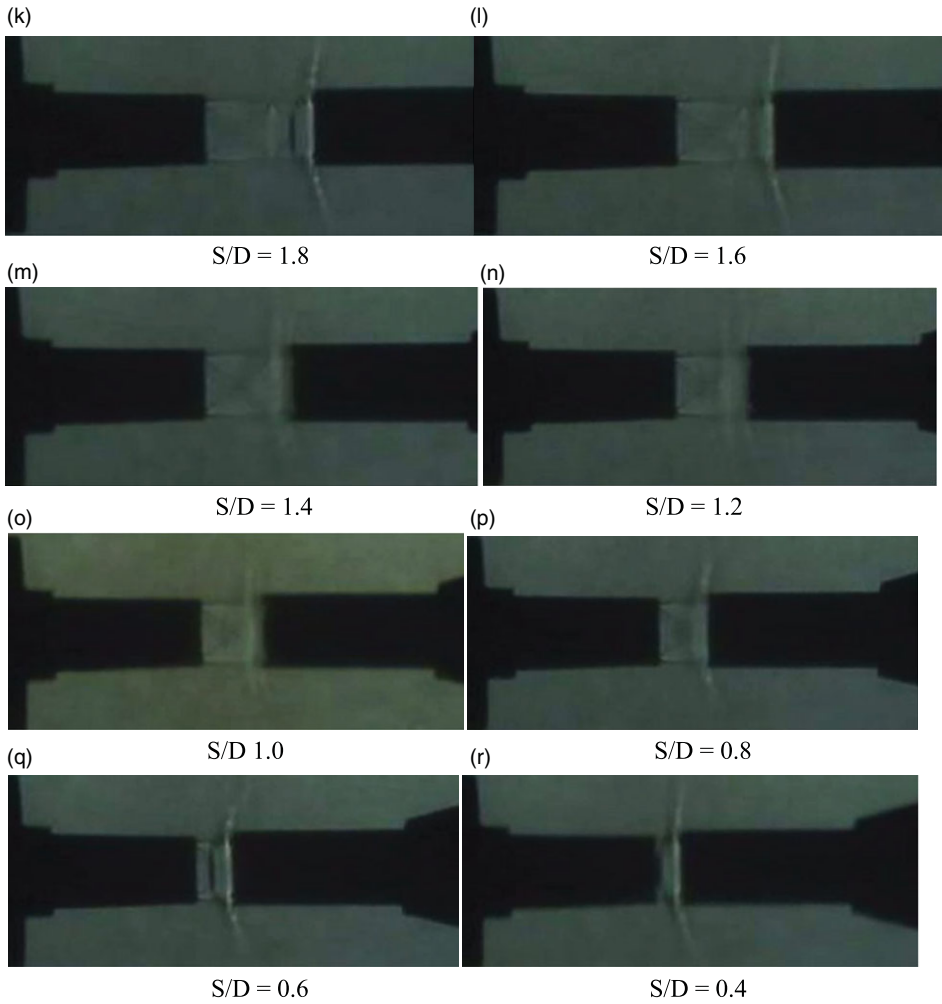


Figure 20. Continued.

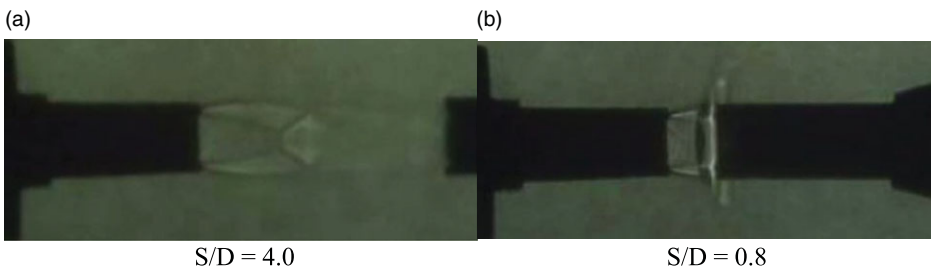


Figure 21. Shadowgraph images for spacing S/D from 4.0 and 0.8 at NPR 5. (a) $S/D=4.0$ and (b) $S/D=0.8$.

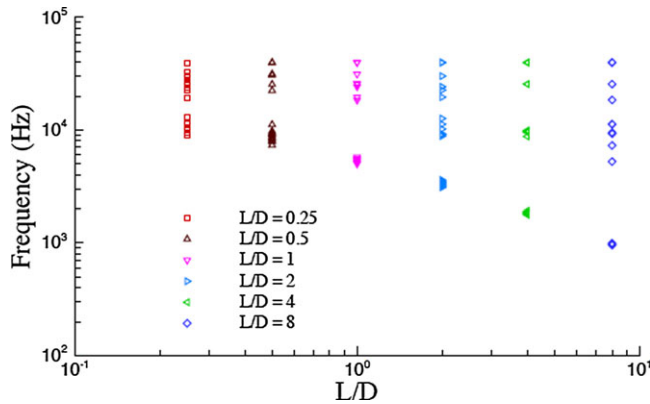


Figure 22. Frequency vs. cavity depth at $S/D = 1$.

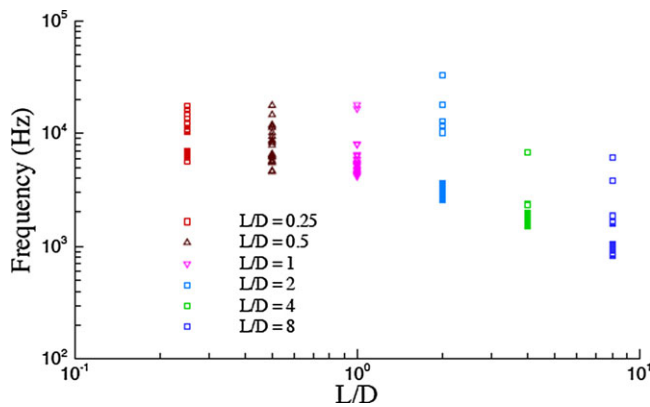


Figure 23. Frequency vs. cavity depth at $S/D = 2$.

tube has been reported in open literature except Smith and Powell [11], and some recent reports by Sarpotdar et al. [16] and Kastner and Samimy [17].

With the aim to extend the range of the studies referred to above, measurements were made of the frequency response, which relates the acoustic output of a typical cavity to the jet pressure (and hence to the jet structure) at spacing $S/D = 1, 2$ and 3 . As can be seen from Fig. 10(b) and 10(c), this spacing corresponds to positions in the first, second and third shock cells, respectively, for moderate NPRs ($3 - 3.5$). The sampling rate employed for the acoustic measurements is 80 kHz. A cut-off of 130 dB is used to consider the discrete tones present in the signal (as it is only the high-amplitude tones that are of interest in the current study).

12.1 Effect of cavity depth

Figures 22-24 show the frequency – L/D relationship, at spacing $1, 2$ and 3 , respectively. From Fig. 22, it can be observed that at any given L/D , there are distinguished frequency bands, concentrated towards the lower and higher values of the spectrum. Sometimes an intermediate band is also present. Careful observation reveals that the higher and intermediate bands are almost independent of the cavity depths i.e. at a given S/D ; the frequencies in higher-end band are the same irrespective of what the tube depth is. These frequencies correspond to screech mode. The lower band corresponds to that of JRG, which shows an inverse relationship with cavity depth. Figure 25 shows the average values of these frequencies

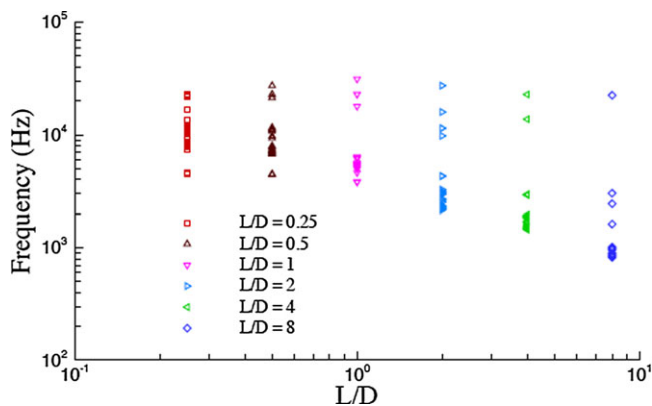


Figure 24. Frequency vs. cavity depth at $S/D = 3$.

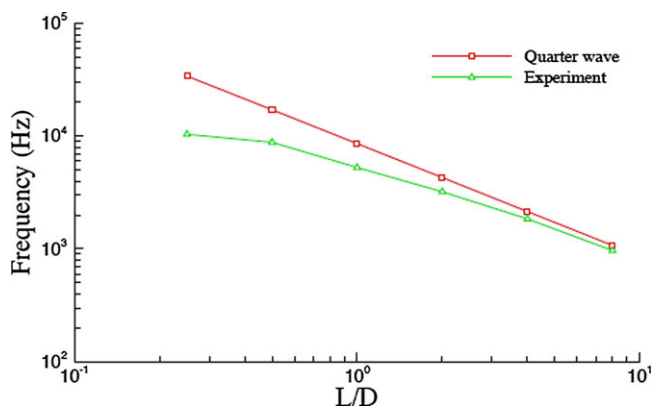


Figure 25. Average frequency (JRG) vs cavity depth at $S/D = 1$.

plotted against the cavity depth. The quarter wave frequencies are also calculated for these depths with reference to ambient stagnation temperature. It is observed that the experimental values approach the calculated values for higher L/D s. This can be expected since quarter wave frequency approximation of the linear acoustic theory is only valid when the fluid inside the cavity is stagnant and the penetration depth of the jet is low which can only be realised for longer tube depths and/or low to moderate NPRs.

12.2 Effect of NPR

As the shock cell length increases with increasing NPR, it is analogous to moving the cavity upstream in the jet. Also, there is a change in shock structure from diamond cell to Mach disk for NPR greater than 4. In Figs. 26–28, the variation of frequency with NPR is presented for S/D 1, 2 and 3.

$S/D = 1$:

Figure 26 shows a frequency response of the tube at spacing $S/D = 1$ by increasing the NPR for different depths of the tube. It can be seen that the response of the tube with NPR is identical for $L/D = 1, 2, 4$ and 8 except near the JRG to screech transition. This point will be discussed in a later section on the transition dependence on L/D . Figure 11 shows the variation of locations of cross-over points and terminations of the individual cells with NPR. It can be noted that, for NPR between 2 to about

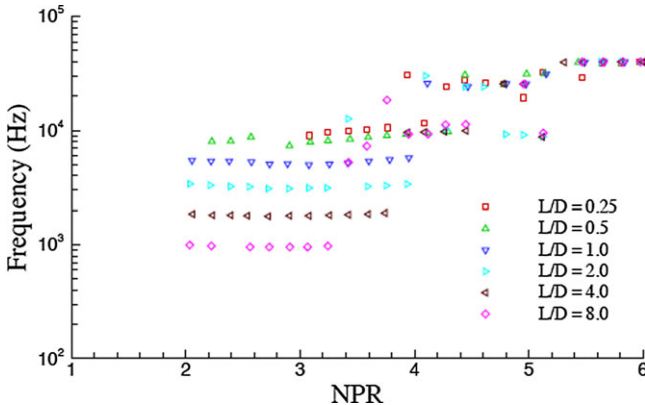


Figure 26. Frequency (JRG) vs. NPR at S/D = 1.

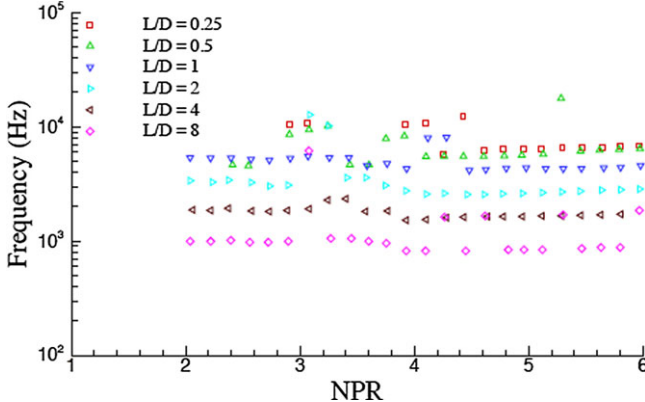


Figure 27. Frequency (JRG) vs. NPR at S/D = 2.

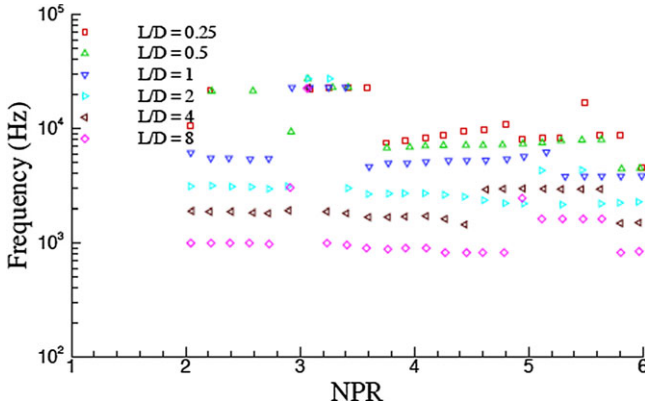


Figure 28. Frequency (JRG) vs. NPR at S/D = 3.

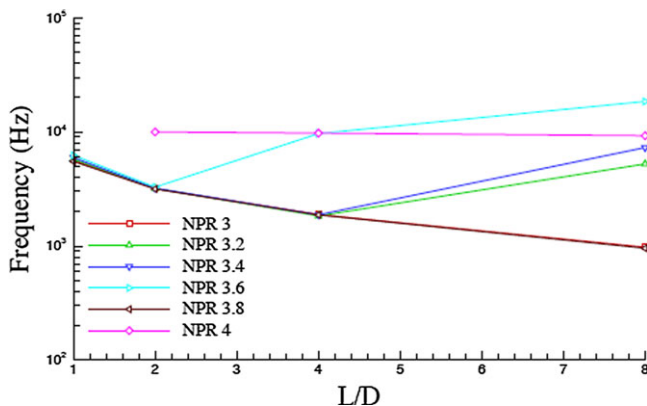


Figure 29. Transition dependence on L/D .

3.2, the $S/D = 1$ position corresponds to cavity positions centred around the maxima of the pitot pressure curve. Therefore, as discussed before, this range corresponds to operating in the JRG. This figure (Fig. 26) also shows that the operating range of JRG can be increased by reducing the cavity depth (thereby restricting the axial movement of the interface). Beyond this point, the tube is operating in the screech mode. Also noted here is that the screech mode is independent of NPR. This is justified because in that range the cavity is already into the expansion region of the first shock cell, the standoff shock movement is not appreciable from the cavity by increasing the NPR. As proposed by Morch [10], since screech mode frequencies primarily depend on the distance from the standoff shock to the cavity, the frequency is more or less the same. For shorter cavity depths (0.25 and 0.5), however, the trend is such that the frequency is increasing with NPR.

$S/D = 2$ and 3:

For NPR greater than 4, every position after the first cell (S/D s 2 and 3 are way beyond the first cell as can be seen in Fig. 11) corresponds to operation in JRG, the frequency is almost independent of the NPR. Between NPRs 2.5 to 3, it is in JRG (cavity centred around maxima corresponding to the 2nd and 3rd cell) between 3 to 4, cavity located at spacing $S/D = 2$, undergoes a transition at cell 2 cross-over point (also possibly because of transition from diamond cell to barrel structure of the jet core).

The response of the cavity at $S/D = 3$ is not similar to that at $S/D = 2$. This may possibly be due to the recovery of subsonic flow in the second cell to form cells 3 and beyond which interact with the cavity mouth.

13.0 Transition dependence on the cavity depth

From Fig. 26, it is seen that the transition to screech from JRG appears to depend on the cavity depth. Longer cavities show an early transition to screech than the shorter ones. To confirm this point, tests were performed again between NPRs 3 to 4 (in the intervals of 0.2) at spacing $S/D = 1$. The selected depths of the cavity (L/D) are 1, 2, 4 and 8. Figure 29 shows the corresponding plot obtained in this repeated experiment, where frequencies are plotted against the cavity depth. For NPRs 3 and 3.2, the operational mode is only JRG as can be seen from the inverse relationship with the cavity depth. However, NPRs 3.4 and 3.6 show a transition at $L/D = 4$, where for $L/D = 8$, the frequency is rising indicating the first stage of screech. This transition occurred as early as $L/D = 2$ for NPR 3.8 while for NPR 4 no JRG is observed. This confirms that the JRG-screech transition depends on the cavity depth. A possible explanation for this may be given considering that since the frequency of charging and debouching of the tube can be related to the extent of axial movement of the interface between the jet and tube flow (in

JRG), longer cavities producing low frequencies imply longer times for charging and debouching and so is the amount of axial freedom for the interface. So, longer cavities can push the interface from what initially is an unstable (JRG) zone to a stable zone (screech).

14.0 Comments

From the above discussion, it may be discerned that the mechanism of shock instability in an under-expanded axisymmetric jet directed against a (longer) cavity is the following. When the jet is directed against a tube open at both ends, formation of a standoff shock at the centreline ahead of the tube cannot be expected, as there is no obstruction to the flow. However, there is an oblique shock cone at the cavity lip (blunt lip). In case the farther end is closed, the tube fills up in the initial part. If the flow is stagnant inside, the tube acts as a blunt body and there is a detached (stand-off) shock ahead of the cavity. If this shock is located in the expansion region (falling pressure) of the jet structure, it is stable and the oscillations of this shock are weak. The perturbations (small) in the pressure and velocity field due to the oscillation of shocks travel towards the cavity (subsonic region) and on reflection, if they are in phase with the oscillations of the shock; the oscillations are sustained as in the picture of Morch [10]. This is referred to as screech mode. If the shock however is located in the compression region (rising pressure), it is unstable, the perturbations are large and the finite perturbations created do a forced excitation to the cavity. Under certain conditions, the excitation is such that the charging and re-filling of the cavity accompany it and the oscillation frequency is nearly the same as the quarter wave frequency of the cavity. Though the flow must be subsonic after the normal shock, just after the initial transients of the mass in and outflows due to forced excitation, the final state is that of the picture of the jet regurgitant mode. So, only under restricted conditions that we observe these two forms of oscillations. No oscillations (broadband) exist for the remaining conditions.

15.0 Amplitude response of the Hartmann tube

Hartmann and other earlier researchers concentrated for the most part on increasing the acoustic efficiency of the tube by experimenting with different combinations of geometrical parameters, and also using various forms of acoustic reflectors, etc. Though much of the consideration given in the current investigation is on the spectral content of the signal, limited “trend studies” of the amplitude response are also done. The investigation is “limited” only in the sense of the inability to quantify the exact signal amplitude. The data can however be used if, within the given range of NPRs, irrespective of the acoustic efficiency the combination of geometrical parameters needed to obtain high amplitude tone is to be determined. The experiments were performed by positioning the cavity at a particular spacing (e.g. $S/D = 1$) and by adjusting the piston screw to a particular value of cavity depth. At this combination, the NPR is varied from 2 in increments of 0.2 to 6. This is repeated for all the planned values of cavity depths (0.25, 0.5, 1, 2, 4, 8) after which the entire set is repeated for $S/D = 2$ and 3. However, with the employed cut-off of 130 dB of the microphone signal, all the values less than NPR 2 (subsonic) data are eliminated and only a few of the screech tones are retained. Figures 30-35 show a series of plots constructed to show the amplitude-depth, amplitude-NPR relationships at each of the spacing ($S/D = 1, 2, \text{ and } 3$), respectively. The common picture is that, for higher L/D s, within the range of NPRs tested for the study, the amplitude is decreasing. The maxima however be located at $S/D = 1$ and 2, for $L/D = 1$ ($L/D = 0.5$ also shows a nearly equal value). For $S/D = 3$ however, the maximum amplitude that can be obtained with the range of NPRs operated (between 2 to 6) is observed at $L/D = 0.5$. This result should not be compared with Hartmann’s result that the combination for maximum acoustic efficiency is $S/D = L/D = 1$ as the presented result only indicates the combination to obtain the maximum acoustic output in (dB) without consideration of efficiency. A similar trend is observed with NPR versus amplitude at $S/D = 1$. The maxima observed within the region of NPR 3 - 4 could be seen in Fig. 30.

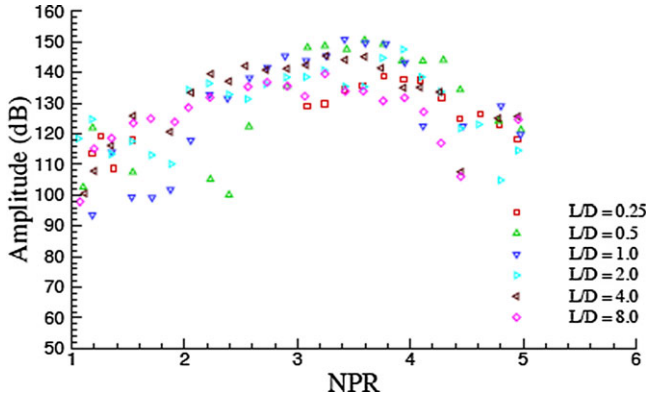


Figure 30. Amplitude variation with NPR for $S/D = 1$.

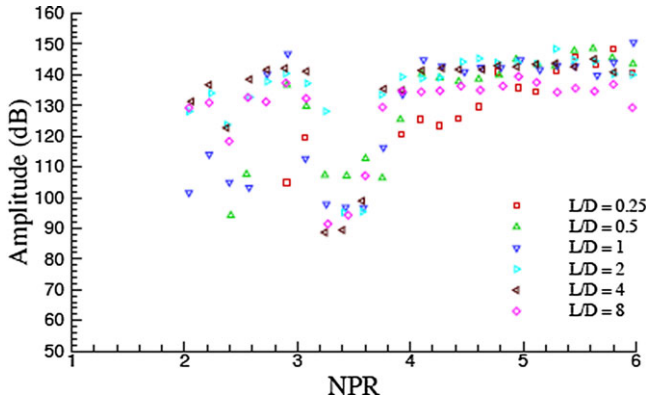


Figure 31. Amplitude variation with NPR for $S/D = 2$.

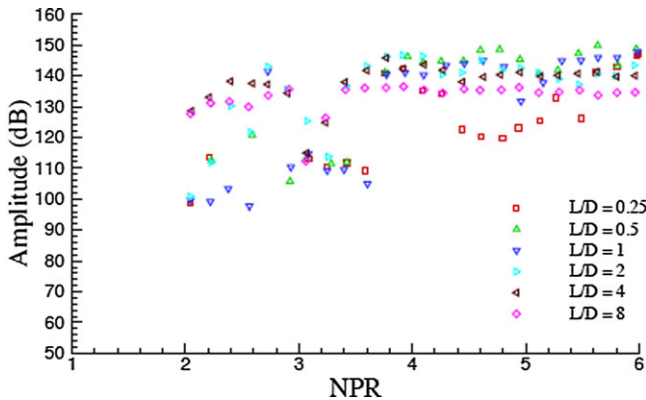


Figure 32. Amplitude variation with NPR for $S/D = 3$.

The maxima are different for different L/D . Also, it is observed that with an increase in NPR, the level of surrounding broadband noise is increasing. Figure 36 shows NPR vs. broadband amplitude operating at spacing $S/D = 1$. The amplitude at for $L/D = 4$, $S/D = 1$, at NPR around 2.2 is off from the mean value. This may be because of the oscillation of the of the flow just behind the first shock-crossover point, similar to that seen in the shadow graph image Fig. 20(o), for NPR 3. An identical pattern was

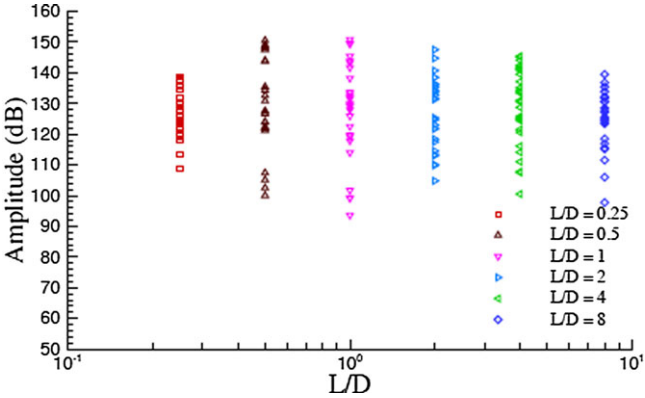


Figure 33. Amplitude variation with L/D for S/D = 1.

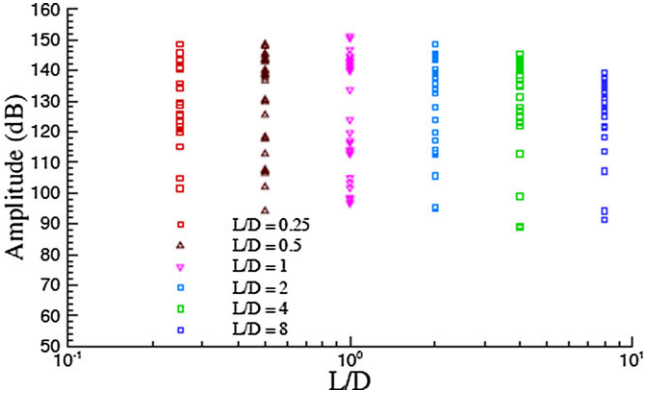


Figure 34. Amplitude variation with L/D for S/D = 2.

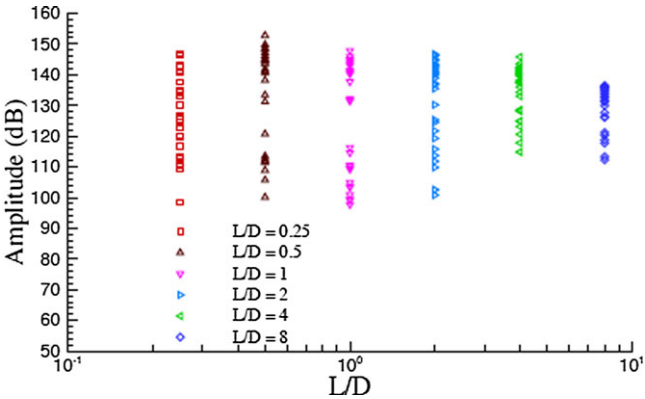


Figure 35. Amplitude variation with L/D for S/D = 3.

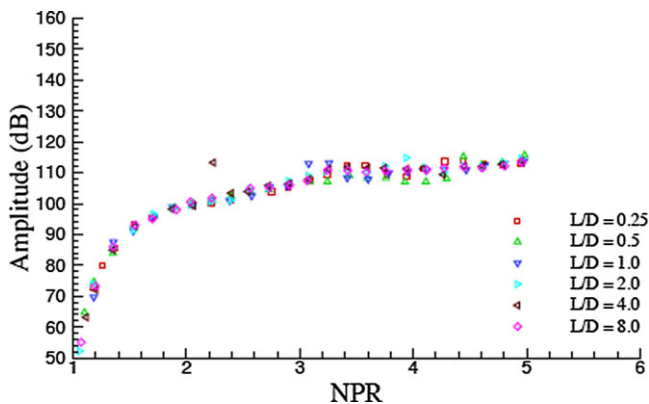


Figure 36. Broadband variation with NPR.

observed for $S/D = 2$ and 3 . This noise as it is independent of the geometric parameters can be attributed to jet noise alone.

16.0 Conclusions

The response of the Hartmann tube is strongly influenced by the free jet shock cell structure. The structure of the jet also is found to influence the operating modes. For lower NPRs (moderate underexpansions), the tube resonates in jet regurgitant mode (JRG) mode, only within some periodic intervals of cavity positions along the jet axis. When correlated with the jet structure, this appears to be around the shock cell termination locations. For higher NPRs, the JRG tones are observed almost for every spacing (S/D) beyond the first shock cell. The standoff shock location ahead of the Hartmann tube in the cell structure plays an important role in the observed modes rather than nozzle-cavity spacing as reported in the majority of literature. It is found to be associated with the instability of shock in rising pressure regions i.e. if the standoff shock is located in the compression region of a shock-cell, the high amplitude discrete tones (the regurgitant mode) are observed, whereas if standoff shock is in the expansion region, high frequency (screach mode) occurs.

In the JRG, the frequency shows an inverse relationship with the cavity depth. The value approached the quarter wave frequency of longer tubes (large L/D).

The screach mode frequencies are found to be independent of the cavity depth (L/D). However, it is found to be strongly dependent on the nozzle pressure ratio and the spacing (S/D). The screach mode is observed in stages, the frequencies rising for each subsequent stage.

The cavity depth is found to influence the transition between the JRG and screach. Longer cavities exhibit early transitions than shorter ones. This is contrary to the available literature. Some trend studies on amplitude characteristics indicate that within the range of NPR (2-6), the observed maximum amplitude occurs at $L/D = 1$ for $S/D = 1$ and 2 . Whereas, for $S/D = 3$, the maxima is found at $L/D = 0.5$.

Acknowledgements. Author sincerely thanks his master's degree student Praveen Throvagunta for conducting the experiments of this study.

References

- [1] Borisov, Y.Y. *Sources of High-Intensity Ultrasound*, Plenum Press, 1968, New York, NY.
- [2] Brocher, E., Maresca, C. and Bournay, M.H. Fluid dynamics of the resonance tube. *J. Fluid Mech.*, 1970, **43**, pp 369–384.
- [3] Brun, E. and Boucher, R.M.G. Research on the acoustic air-jet generator: a new development. *J. Acoustic Soc Am*, 1957, **29**, pp 573–583.
- [4] Chang, S.M. and Lee, S. On the jet regurgitant mode of a resonant tube. *J. Sound Vib*, 2001, **246**, pp 567–581.

- [5] Gravitt, J.C. Frequency response of an acoustic air-jet generator. *J. Acoustic Soc Am*, 1959, **31**, pp 1516–1518.
- [6] Hartmann, J. On a new method for the generation of sound waves. *Physical Rev*, 1919, **20**, pp 719–727.
- [7] Hartmann, J. On the production of acoustic waves by means of an air-jet of a velocity exceeding that of sound. *Phil. Mag.*, 1931, **11**, pp 926–948.
- [8] Savory, L.E. Experiments with the Hartmann acoustic generator. *Eng*, 1950, **170**, pp 136–138.
- [9] Thompson, P.A. Resonance Tube, PhD thesis, Massachusetts Institute of Technology, 1960.
- [10] Morch, K.A. A theory for the mode of operation of the Hartmann air-jet generator. *J. Fluid Mech.*, 1964, **20**, pp 141–159.
- [11] Smith, T. and Powell, A. Experiments concerning the Hartmann whistle, Tech Rep 64–42, University of California, 1964.
- [12] Kawahashi, M. and Suzuki, M. Generative mechanism of air column oscillations in a Hartmann-Sprenger tube excited by an air jet issuing from a convergent nozzle. *J. Appl Math Phys*, 1979, **30**, pp 797–810.
- [13] Sarohia, V. and Back, L.H. Experimental investigation of flow and heating in a resonance tube. *J. Fluid Mech.*, 1979, **94**, pp 649–672.
- [14] Jungowski, W.M. and Grabitz, G. Self-sustained oscillation of a jet impinging upon a Helmholtz resonator. *J. Fluid Mech.*, 1987, **179**, pp 77–103.
- [15] Iwamoto, J. and Dekker, B.E.L. A study of the Hartmann tube using the hydraulic analogy. *Exp Fluids*, 1985, **3**, pp 245–252.
- [16] Sarpotdar, S., Raman, G. and Cain, A.B. Powered resonance tubes: resonance characteristics and actuation signal directivity. *Exp Fluids*, 2005, **39**, pp 1084–1095.
- [17] Kastner, J. and Samimy, M. Development and characterization of Hartmann tube fluidic actuators for high-speed flow control. *AIAA J.*, 2002, **40**, pp 1926–1934.
- [18] Thomas, S.K., Narava, V.S.R. and Srinivasan, K. Role of non-circular jets in the performance of Hartmann whistles. *Appl Acoust*, 2022, **192**, pp 108736.
- [19] Solomon, J.T., Lockyer, R., Jones, T. and Kreth, P. High-frequency pulsed coaxial injectors for high-speed flow mixing and control. *AIAA J*, 2030, **61**, pp 1–15.
- [20] Rathakrishnan, E. *Applied Gas Dynamics* 2nd ed. Wiley, 2019.